

Structural and magnetic properties of stage-2 $\text{Co}_c\text{Mn}_{1-c}\text{Cl}_2$ -graphite intercalation compounds

Itsuko S. Suzuki, Masatsugu Suzuki, Li-Fen Tien, and Charles R. Burr

*Department of Physics and Materials Research Center, State University of New York at Binghamton,
Binghamton, New York 13902-6000*

(Received 27 August 1990)

Stage-2 $\text{Co}_c\text{Mn}_{1-c}\text{Cl}_2$ -graphite intercalation compounds ($0 \leq c \leq 1$) are two-dimensional random-spin systems with competing ferromagnetic and antiferromagnetic exchange interactions. The structural and magnetic properties of these compounds for $0 \leq c \leq 1$ have been studied by x-ray diffraction and dc magnetic susceptibility. An analysis of the (00L) x-ray diffraction using a simple model developed here shows that these compounds are dominantly stage 2 but have a Hendricks-Teller-type staging disorder along the c axis. The c -axis repeat distance is proportional to the Co concentration, suggesting that both Co and Mn ions are randomly distributed on the triangular lattice of the $\text{Co}_c\text{Mn}_{1-c}\text{Cl}_2$ intercalate layers. The phase diagram determined from the dc magnetic susceptibility exhibits a ferromagnetic phase for $0.45 \leq c \leq 1.0$. The Curie-Weiss temperature increases monotonically with increasing Co concentration. Its sign changes from negative to positive around $c \approx 0.2$. The exchange interaction between Co and Mn spins is ferromagnetic and is described by $J(\text{Co-Mn}) = 1.2 [|J(\text{Co-Co}) J(\text{Mn-Mn}) |]^{1/2} = 1.49$ K. The average effective magnetic moment shows a minimum around $c \approx 0.3$, suggesting a partial replacement of Mn^{2+} ions by Mn^+ or Mn^{3+} ions because of a charge transfer.

I. INTRODUCTION

Recently magnetic phase transitions of magnetic graphite intercalation compounds (GIC's) such as CoCl_2 and NiCl_2 GIC have received considerable interest because of their two-dimensional nature.¹⁻³ In magnetic GIC's with stage number N , the magnetic intercalate layer can be separated by N graphite layers. The interplanar exchange interaction J' between spins in adjacent magnetic intercalate layers is greatly reduced as the stage number increases. The ratio of the interplanar exchange interaction $|J'|$ to the intraplanar exchange interaction J between spins in the same layers is on the order of 10^{-4} for the stage-2 CoCl_2 GIC.⁴

The effective interplanar exchange interaction J'_{eff} between spins over the in-plane spin correlation length ξ_{\perp} in adjacent magnetic layers can be described in terms of $J'_{\text{eff}} = J'(\xi_{\perp}/a)^2$, where a is the in-plane lattice constant. For quasi-two-dimensional (2D) magnetic systems such as Rb_2CoF_4 , the in-plane spin-correlation length ξ_{\perp} divergently increases as the temperature approaches a critical temperature T_c . Once 2D spin ordering occurs in the same layer, it gives rise to 3D ordering simultaneously through the effective interplanar exchange interaction even if $|J'|$ is very small compared to J . The spin-ordering process in CoCl_2 and NiCl_2 GIC is very different from that in such quasi-2D magnetic systems. In these compounds the magnetic intercalate layers are formed of small islands, which is a common feature to the acceptor type GIC's. The island size is typically on the order of 500 Å. The boundary of these islands provides acceptor sites for electrons which are transferred from the graphite π band. The growth of ξ_{\perp} is limited by the island size as the temperature is decreased. Suppression of the in-

crease of J'_{eff} leads to the realization of 2D spin ordering between T_{cl} ($=8.0$ K) and T_{cu} ($=9.1$ K) for stage-2 CoCl_2 GIC. Below T_{cl} there occurs 3D spin ordering where the 2D ferromagnetic layers are antiferromagnetically stacked along the c axis.⁴ There has been a recent report by Speck and Dresselhaus⁵ that the structural correlation length in the CoCl_2 intercalate layer is much larger than 500 Å. In the case when ξ_{\perp} is much larger than $a(J/J')^{1/2}$ and is smaller than the structural correlation length, it is predicted from the above model that the 2D ordered phase between T_{cl} and T_{cu} does not occur.

The magnetic GIC's described above are called magnetic binary GIC's where only one magnetic intercalant species is included in the intercalate layers. The magnetic ternary GIC's with two kinds of magnetic intercalant species introduced into the same galleries of the host graphite provide a variety of opportunities to study magnetic phase transitions of 2D random-spin systems. There have been several studies on magnetic properties of magnetic ternary GIC's such as stage-2 $\text{Co}_c\text{Ni}_{1-c}\text{Cl}_2$ GIC's and stage-1 $\text{Co}_c\text{Mg}_{1-c}\text{Cl}_2$ GIC's where c is the Co concentration ($0 \leq c \leq 1.0$). Yeh *et al.*^{6,7} have reported the first successful results on dc magnetic susceptibility of stage-2 $\text{Co}_c\text{Ni}_{1-c}\text{Cl}_2$ GIC's, where the intraplanar exchange interaction between Co^{2+} and Co^{2+} spins is ferromagnetic and the intraplanar exchange interaction between Ni^{2+} and Ni^{2+} spins is also ferromagnetic. Nicholls and Dresselhaus⁸ have studied the dilution effect of the magnetic phase transition of the stage-1 CoCl_2 GIC with nonmagnetic impurity MgCl_2 by the temperature and field dependences of ac magnetic susceptibility.

The stage-2 $\text{Co}_c\text{Mn}_{1-c}\text{Cl}_2$ GIC's ($0 \leq c \leq 1$) provide a model system for studying the phase transition of the 2D

random-spin systems which is very different from that of stage-2 $\text{Co}_c\text{Ni}_{1-c}\text{Cl}_2$ GIC's and stage-1 $\text{Co}_c\text{Mg}_{1-c}\text{Cl}_2$ GIC's. In the stage-2 $\text{Co}_c\text{Mn}_{1-c}\text{Cl}_2$ GIC's,⁹ Co^{2+} and Mn^{2+} ions are randomly distributed within the same intercalate layer. The intraplanar exchange interaction between Co^{2+} and Co^{2+} spins is ferromagnetic, while the intraplanar exchange interaction between Mn^{2+} and Mn^{2+} spins is antiferromagnetic. The competition between ferromagnetic and antiferromagnetic interactions is expected to give rise to a spin-glass phase at low temperature.¹⁰

The structural properties of the stage-2 $\text{Co}_c\text{Mn}_{1-c}\text{Cl}_2$ GIC's have been investigated using (00L) x-ray diffraction at 300 K. For the ideal case when the Co and Mn atoms are randomly distributed in the intercalate layer, the d spacing is expected to be proportional to the Co concentration. The c -axis repeat distance of the stage-2 $\text{Co}_c\text{Mn}_{1-c}\text{Cl}_2$ GIC's is determined as a function of the Co concentration, and is compared to the empirical Vegard law. In these compounds, the graphite layer and the $\text{Co}_c\text{Mn}_{1-c}\text{Cl}_2$ intercalate layer are weakly coupled to each other by an attractive Coulomb interaction through a small amount of charge transfer. This leads to a Hendricks-Teller (HT) -type staging disorder along the c axis. The (00L) x-ray diffraction pattern of GIC's with HT-type staging disorder¹¹ are characterized by (i) the peak shift (PS) of Bragg reflections from that of pure stage and (ii) the full width at half maximum (FWHM) of Bragg reflections which depends on the index of Bragg reflections. The PS and FWHM of the (00L) Bragg reflections observed in the x-ray diffraction of the stage-2 $\text{Co}_c\text{Mn}_{1-c}\text{Cl}_2$ GIC's are discussed in terms of a simple theory developed in Sec. III.

The magnetic properties of these compounds have been investigated by dc magnetic susceptibility in the temperature range between 1.5 and 300 K. The Curie-Weiss temperature and the effective magnetic moment are determined as a function of the Co concentration, and discussed in terms of the molecular-field theory. The variation of the dc magnetic susceptibility with temperature is found to show a considerable rounding of the transition. The average critical temperature is determined as a function of the Co concentration by assuming a Gaussian distribution of the critical temperature. We show that there is no direct evidence of a spin-glass phase from the dc magnetic susceptibility.

II. BACKGROUND: MAGNETIC PROPERTIES

The spin Hamiltonian of Co^{2+} in the stage-2 CoCl_2 GIC can be expressed as^{4,12}

$$\mathcal{H} = -2J \sum_{\langle i,j \rangle} \mathbf{S}_i \cdot \mathbf{S}_j + 2J_A \sum_{\langle i,j \rangle} S_i^z S_j^z + 2J' \sum_{\langle i,m \rangle} \mathbf{S}_i \cdot \mathbf{S}_m, \quad (1)$$

where the z axis coincides with the c axis, $\langle i,j \rangle$ denotes nearest-neighbor pairs on the same intercalate layer, $\langle i,m \rangle$ denotes nearest-neighbor pairs on the adjacent intercalate layer, S is a fictitious spin ($S = \frac{1}{2}$) of Co^{2+} , J is the intraplanar exchange interaction ($J = 7.75$ K), J_A is

TABLE I. Structural and magnetic properties of stage-2 CoCl_2 and MnCl_2 GIC, where a is the in-plane lattice constant and d is the c -axis repeat distance.

stage-2 CoCl_2 GIC		stage-2 MnCl_2 GIC	
a (Å)	3.55	a (Å)	3.67
d (Å)	12.79	d (Å)	12.89
S	$\frac{1}{2}$	S	$\frac{5}{2}$
g value	6.4	g value	2.04
J (K)	7.75	J (K)	-0.20
J_A (K)	3.72	D	0.97
T_{cl} (K)	8.0	T_N (K)	1.1
T_{cu} (K)	9.1		
Θ (K)	23.2	Θ (K)	-10.19
P_{eff} (μ_B /mol)	5.54	P_{eff} (μ_B /mol)	6.04

the anisotropic exchange interaction showing XY anisotropy because of $J_A > 0$ ($J_A/J = 0.48$), and J' is the antiferromagnetic interplanar exchange interaction. The interplanar exchange interaction is very small compared to the intraplanar exchange interaction: $|J'(\text{Co-Co})/J(\text{Co-Co})| = 8 \times 10^{-4}$. The effective magnetic moment of the Co^{2+} ion is given by $P(\text{Co}) = g[S(S+1)]^{1/2} = 5.54 \mu_B/\text{mol}$ for $S = \frac{1}{2}$ and $g = 6.40$. The c -axis repeat distance is 12.79 Å and the in-plane lattice constant is $a = 3.55$ Å. The magnetic and structural data of this compound are listed in Table I. This compound shows two magnetic phase transitions at $T_{\text{cu}} = 9.1$ K and $T_{\text{cl}} = 8.0$ K. Above T_{cu} , the system is in the paramagnetic phase. In the intermediate phase between T_{cl} and T_{cu} the system has 2D spin ordering. There is no spin correlation between adjacent CoCl_2 layers. Below T_{cl} , there occurs the 3D antiferromagnetic phase where the 2D ferromagnetic layers are antiferromagnetically stacked along the c axis. The stage-2 CoCl_2 GIC magnetically behaves like a 2D XY ferromagnet on the triangular lattice sites.

The spin Hamiltonian of Mn^{2+} ions in the stage-2 MnCl_2 GIC can be expressed by¹²

$$\mathcal{H} = -2J \sum_{\langle i,j \rangle} \mathbf{S}_i \cdot \mathbf{S}_j + D \sum_i (S_i^z)^2 + 2J' \sum_{\langle i,m \rangle} \mathbf{S}_i \cdot \mathbf{S}_m, \quad (2)$$

where $S = \frac{5}{2}$, J is the antiferromagnetic intraplanar exchange interaction, D is the single ion anisotropy parameter, and J' is the interplanar exchange interaction; $J(\text{Mn-Mn}) = -0.2$ K and $D(\text{Mn-Mn}) = 0.97$ K. The single-ion anisotropy constant D is positive, indicating XY anisotropy. The effective magnetic moment of the Mn^{2+} ion is given by $P(\text{Mn}) = g[S(S+1)]^{1/2} = 6.04 \mu_B/\text{mol}$ for $S = \frac{5}{2}$ and $g = 2.04$. The c -axis repeat distance is 12.89 Å and the in-plane lattice constant is $a = 3.67$ Å. The magnetic and structural data of this compound are shown in Table I. This compound shows a magnetic phase transition at $T_N = 1.1$ K.^{13,14} Above T_N , it is in the paramagnetic phase. Below T_N , it is in the antiferromagnetic phase where all spins lie in the MnCl_2 layers. This compound behaves magnetically like a 2D XY antiferromagnet on the triangular lattice sites.

III. MODEL: (00L) X-RAY DIFFRACTION AND STAGING DISORDER

The effect of the HT staging disorder on the (00L) x-ray scattering intensity of GIC's has been discussed in detail by Hohlwein and Metz¹⁵ for FeCl₃ GIC's, and Huster *et al.*¹⁶ for K GIC's. Here we present a simple theory of the (00L) x-ray scattering intensity for the Co_cMn_{1-c}Cl₂ GIC's with a HT-type staging disorder. According to the theory first proposed by Hendricks and Teller,¹¹ and subsequently modified by Kakinoki and Komura,¹⁷ the x-ray scattering intensity along $Q = (00Q_c)$ can be expressed in terms of matrix representation as

$$I(Q) = \text{Tr} \left[\underline{F} \underline{V} \frac{1}{1 - \underline{P}\underline{\Phi}} \right] + \text{Tr} \left[\underline{F} \underline{V}^* \frac{1}{1 - \underline{P}\underline{\Phi}} \right] - \text{Tr}(\underline{F} \underline{V}). \quad (3)$$

The matrices \underline{F} and $\underline{\Phi}$ have only diagonal elements expressed by $F_{rs} = f_r \delta_{rs}$ and $\Phi_{rs} = \phi_r \delta_{rs}$, where δ_{rs} is the Kronecker delta function and f_r is the probability of finding the package with stage r ($r = 1, 2, 3, \dots$). The phase factor ϕ_r is defined by

$$\phi_r(Q_c) = e^{iQ_c[2c_1 + c_2(r-1)]}, \quad (4)$$

where $2c_1$ is the distance between adjacent graphite layers with the gallery occupied by the Co_cMn_{1-c}Cl₂ intercalate layer, and c_2 is the distance between adjacent graphite layers without the intercalate layer. Note that the package with stage 3 denotes the layered sandwich structures of $G-I-G-G-G$ along the c axis, where G and I denote the graphite layer and the intercalate layer. The matrix element of \underline{P} , P_{rs} , is the transition probability of finding the package with stage r next to the package with stage s . The matrix element of \underline{V} is expressed by $V_{rs} = V_r^* V_s$, where V_s is the structure form factor of the package with stage s and is given by

$$\begin{aligned} V_s(Q_c) = & [\rho_{\text{Co}} f_{\text{Co}}(Q_c) + \rho_{\text{Mn}} f_{\text{Mn}}(Q_c) \\ & + 2\rho_{\text{Cl}} f_{\text{Cl}}(Q_c) \cos(z_1 Q_c)] e^{-i(Q_c c_1)} \\ & + \rho_G f_G(Q_c) \sum_{k=1}^s e^{i[Q_c(k-1)c_2]}, \end{aligned} \quad (5)$$

where z_1 is the distance between the Co_cMn_{1-c} layer and the Cl layer, and $f_i(Q_c)$ is the atomic form factor of i atom ($i = \text{Co}, \text{Mn}, \text{Cl}, \text{and C}$). The number of i atoms per unit area ρ_i is given by

$$\rho_G = \frac{n}{\sum_r f_r}, \quad \rho_{\text{Cl}} = \frac{2+\delta}{2}, \quad \rho_{\text{Co}} = c, \quad \rho_{\text{Mn}} = 1-c \quad (6)$$

for the stoichiometry $C_n \text{Co}_c \text{Mn}_{1-c} \text{Cl}_{2+\delta}$, where δ is the number of extra chlorine atoms.

The x-ray scattering intensity depends on the details of the transition probability P_{rs} . For $P_{rs} = \delta_{rs}$ corresponding to complete phase separation, the intensity is simply given by

$$I(Q_c) = \sum_r f_r |V_r|^2 \delta(\phi_r(Q_c) - 1), \quad (7)$$

where $\delta(x)$ is a Dirac delta function. This result indicates that the Bragg reflection with the intensity $f_r |V_r|^2$ is located at $Q_c = L(2\pi/d_r)$, where L is an integer, and d_r is the c -axis repeat distance of the stage- r Co_cMn_{1-c}Cl₂ GIC and is given by $d_r = 2c_1 + (r-1)c_2$. For $P_{rs} = f_r$ corresponding to a completely random distribution, the intensity is given by

$$\begin{aligned} I(Q_c) = & \sum_r f_r |V_r|^2 + \frac{1}{1 - \sum_r \phi_r f_r} \left[\sum_s \phi_s f_s V_s^* \right] \left[\sum_t V_t f_t \right] \\ & + \frac{1}{1 - \sum_r \phi_r^* f_r} \left[\sum_s \phi_s^* f_s V_s \right] \left[\sum_t V_t^* f_t \right]. \end{aligned} \quad (8)$$

For simplicity, here we consider a system consisting of stage-1, stage-2, and stage-3 packages with the fractions of f_1 , f_2 , and f_3 , respectively, where $f_1 + f_2 + f_3 = 1$. These packages are assumed to be randomly distributed along the c axis. In the case when $f_2 > f_1 + f_3$, the (00L) x-ray intensity is predicted to consist of a single set of Bragg reflections of stage 2. The full width at half maximum Δ_{FWHM} of each Bragg peak and the peak shift Δ_{PS} of each Bragg reflection from that of pure stage 2 given by $Q_c = (2\pi L/d)$ are theoretically derived as¹⁸

$$\Delta_{\text{FWHM}} = 2 \frac{f_1 + f_3}{f_2 d} \left[1 - \cos \left[\frac{2\pi L c_2}{d} \right] \right] \quad (9)$$

and

$$\Delta_{\text{PS}} = \frac{f_1 - f_3}{f_2 d} \sin \left[\frac{2\pi L c_2}{d} \right], \quad (10)$$

in the limit of $f_2 \approx 1$ and $f_1 + f_3 \approx 0$, where L is the Bragg index number of stage 2, and d is the c -axis repeat distance of stage 2 given by $d = 2c_1 + c_2$. The Δ_{FWHM} and Δ_{PS} are found to oscillate with L . The amplitude of these oscillations does not depend on the details of the x-ray structure factor. The values of f_1 , f_2 , and f_3 are uniquely determined from the oscillation amplitudes of the Δ_{FWHM} and Δ_{PS} described by Eqs. (9) and (10).

The numerical calculations of the (00L) x-ray intensity for the Co_cMn_{1-c}Cl₂ GIC's were carried out for more general cases of $f_2 > f_1 + f_3$. Since the atomic structure factor of Co is almost the same as that of Mn, the L dependence of PS and FWHM for the (00L) x-ray intensity is assumed to be independent of the Co concentration. Here we show only the results of (00L) x-ray intensity calculation for the Co_cMn_{1-c}Cl₂ GIC's system with $n = 10.85$, $c = 0$, $z_1 = 1.39 \text{ \AA}$, $d = 12.789 \text{ \AA}$, and $\delta = 0.48$ in the following two cases: (i) a mixture of stage-1 and stage-2 packages ($f_1 + f_2 = 1$, $f_1 < f_2$, and $f_3 = 0$), and (ii) mixture of stage-2 and stage-3 packages ($f_2 + f_3 = 1$, $f_3 < f_2$, and $f_1 = 0$). Figure 1 shows the L dependence of (a) FWHM and (b) PS for the CoCl₂ GIC system with a stage-1 and -2 mixture, where L is the index of stage 2. Figure 2 shows the L dependence of (a) FWHM and (b) PS for the CoCl₂ GIC system with a stage-2 and -3 mixture. We find from Figs. 1(a) and 2(a) that for both cases (i) the FWHM has local minima at $L = 4$ and 8, and local

maxima at $L=2$ and 6; and (ii) the value of local maxima at $L=2$ and 6 decreases as f_2 increases. The local minima at $L=4$ and 8 are related to the fact that strong Bragg reflections from stage 1 and stage 3 are almost superimposed on strong Bragg peaks at $L=4$ and 8 of stage

2. The L dependence of Δ_{FWHM} with $f_2 > 0.85$ for both cases is well described by Eq. (9). It is also found from Figs. 1(b) and 2(b) that the PS oscillates with L for both cases. The amplitude of the PS oscillations decreases as f_2 increases for both cases. The phase of the oscillation

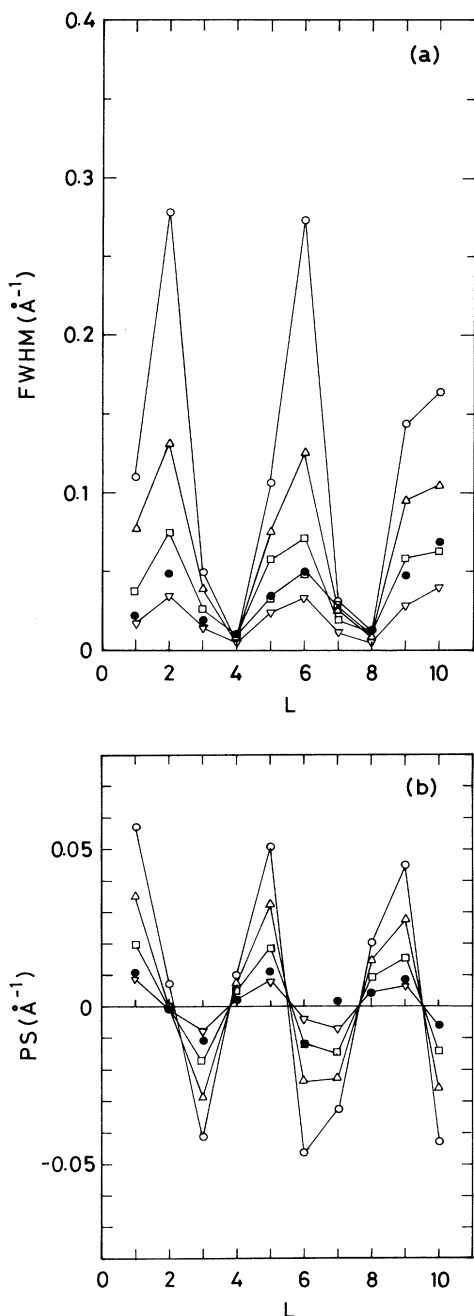


FIG. 1. Model calculations of (a) FWHM and (b) PS for the CoCl_2 GIC system with a stage 1 (f_1) and stage 2 (f_2) mixture, as a function of the Bragg index of stage 2, L : $f_1=0.4, f_2=0.6$ (○); $f_1=0.3, f_2=0.7$ (Δ); $f_1=0.2, f_2=0.8$ (□); and $f_1=0.1, f_2=0.9$ (∇). The closed circles (●) denote the data of the intrinsic FWHM and PS for the sample with $c=1.0$.

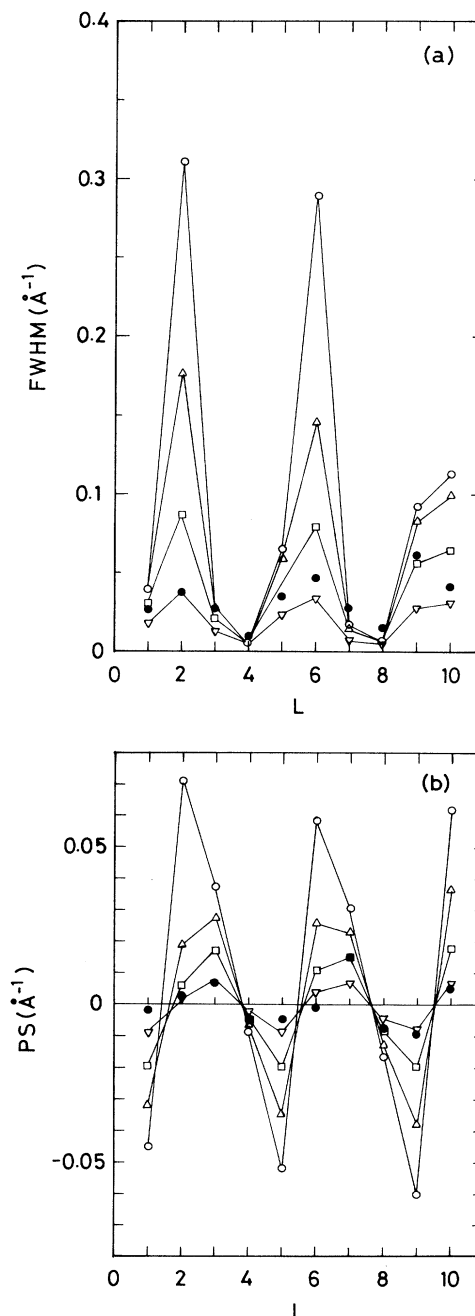


FIG. 2. Model calculations of (a) FWHM and (b) PS for the CoCl_2 GIC system with a stage-2 (f_2) and stage-3 (f_3) mixture, as a function of the Bragg index of stage 2, L : $f_2=0.6, f_3=0.4$ (○); $f_2=0.7, f_3=0.3$ (Δ); $f_2=0.8, f_3=0.2$ (□), and $f_2=0.9, f_3=0.1$ (∇). The closed circles (●) denote the data of the intrinsic FWHM and PS for the sample with $c=0.4$.

TABLE II. Characterization of stage-2 $\text{Co}_c\text{Mn}_{1-c}\text{Cl}_2$ GIC's samples with stoichiometry $\text{C}_n\text{Co}_c\text{Mn}_{1-c}\text{Cl}_2$, where d is the c -axis repeat distance; and f_1, f_2 , and f_3 are the occupation probability of stage 1, 2, and 3, respectively. Sample No. CM55 shows a phase separation of stage 2 and stage 1.

Sample	c	n	d (Å)	f_1	f_2	f_3
No. CM00	0.0	11.03	12.893±0.036	0	0.9	0.1
No. CM05	0.05	10.39	12.848±0.058	0	0.85	0.15
No. CM10	0.10	13.48	12.847±0.027	0	0.8	0.2
No. CM20	0.20	12.95	12.878±0.064	0	0.8	0.2
No. CM25	0.25	9.03	12.871±0.034	0.05	0.95	0
No. CM40	0.40	10.01	12.809±0.036	0	0.85	0.15
No. CM50	0.50	12.67	12.833±0.066	0	0.80	0.20
No. CM55	0.55	10.15	12.814±0.015			
No. CM60	0.60	11.35	12.806±0.241	0	0.6	0.4
No. CM70	0.70	11.00	12.796±0.058	0	0.8	0.2
No. CM85	0.85	10.49	12.792±0.036	0	0.9	0.1
No. CM90	0.90	9.55	12.787±0.026	0	1	0
No. CM100	1.00	9.59	12.789±0.013	0.1	0.9	0

of Δ_{ps} for the stage 1 and 2 mixture [Fig. 1(b)] is different from that for the stage-2 and -3 mixture [Fig. 2(b)] by π , as is well described by Eq. (10) in the limit of $f_2 \approx 1$. This feature is used to determine whether samples consist of a stage-1 and -2 mixture or a stage-2 and -3 mixture.

IV. EXPERIMENT

Single crystals of $\text{Co}_c\text{Mn}_{1-c}\text{Cl}_2$ as intercalants were prepared by heating a mixture of c CoCl_2 and $1-c$ MnCl_2 in vacuum at reaction temperatures depending on the Co concentration: $T = 650^\circ\text{C}$ ($c = 0.1$) (-730°C) ($c = 0.95$). Stage-2 $\text{Co}_c\text{Mn}_{1-c}\text{Cl}_2$ GIC's were synthesized by heating single-crystal Kish graphites and single crystal $\text{Co}_c\text{Mn}_{1-c}\text{Cl}_2$ in a chlorine gas atmosphere with a pressure of 740 Torr. The reaction was continued at 500°C for 20 days. The stoichiometry of GIC samples listed in Table II was determined from a weight uptake measurement.

The (00L) x-ray diffraction of the stage-2 $\text{Co}_c\text{Mn}_{1-c}\text{Cl}_2$ GIC's was measured at 300 K by using a Huber double circle diffractometer with a Mo $K\alpha$ x-ray radiation source (1.5 kW) and a highly oriented pyrolytic graphite monochromator. An entrance slit of $2 \times 2 \text{ mm}^2$ was placed between the monochromator and the sample. The x-ray beam diffracted by the sample was collimated by the exit slit of $1 \times 1 \text{ mm}^2$ and detected by a Bicron photomultiplier tube. The dc magnetic susceptibility of stage-2 $\text{Co}_c\text{Mn}_{1-c}\text{Cl}_2$ GIC's was measured by the Faraday balance method in the temperature range between 1.5 and 300 K. The magnetic field of $100 \leq H \leq 4 \text{ kOe}$ was applied to an arbitrary direction in the c plane of the stage-2 $\text{Co}_c\text{Mn}_{1-c}\text{Cl}_2$ GIC samples.

V. RESULTS AND DISCUSSION

A. (00L) x-ray diffraction

The (00L) x-ray diffraction of the stage-2 $\text{Co}_c\text{Mn}_{1-c}\text{Cl}_2$ GIC's with $0 \leq c \leq 1.0$ was investigated at 300 K. A typi-

cal example of the (00L) x-ray diffraction pattern is shown in Fig. 3 for $c = 0.25$ (No. CM25) as a function of the scattering wave vector Q_c . Sharp Bragg peaks are observed around the Q_c values for stage 2. The peak value Q_c and the full width at half maximum ΔQ_c of each (00L) Bragg peak ($L = 1, 2, \dots, 19$) was determined from the least-squares fit of the data on x-ray intensity versus Q_c to the theoretical curve expressed by a sum of Gaussian distribution and quadratic background. Note that this FWHM is not an intrinsic FWHM which can be obtained from a deconvolution of the measured x-ray intensity with the instrumental resolution function. Figure 4(a) shows the L dependence of the FWHM at 300 K for the stage-2 $\text{Co}_c\text{Mn}_{1-c}\text{Cl}_2$ GIC's with $c = 0, 0.1, 0.7$, and 0.85 , where L is the Bragg index number of stage 2. Most of the FWHM's show local minima at $L = 4$ and 8, and local maxima at $L = 2$ and 6. The value of the local maxima at $L = 2$ and 6 is found to be different for different

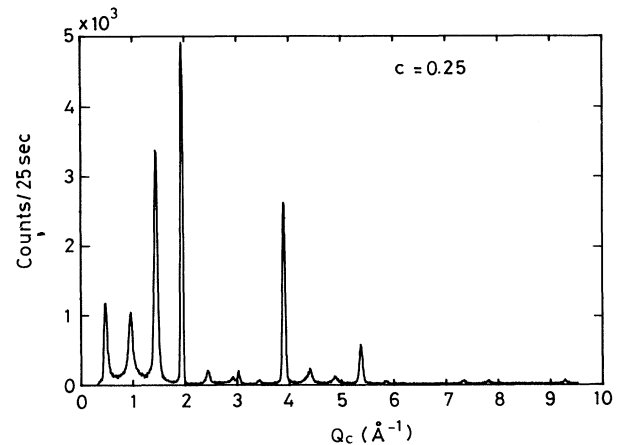


FIG. 3. (00L) x-ray diffraction pattern of stage-2 $\text{Co}_c\text{Mn}_{1-c}\text{Cl}_2$ GIC with $c = 0.25$ at 300 K. $Q_c = L(2\pi/d)$ with $d = 12.871 \text{ Å}$.

samples. For simplicity we assume that the intrinsic FWHM is obtained by subtracting the minimum value of FWHM at $L = 4$ ($=0.05 \text{ \AA}^{-1}$) from the FWHM. The intrinsic FWHM for $c = 1.0$ and 0.4 thus obtained is shown in Figs. 1(a) and 2(a), respectively, for comparison with calculations.

Figure 4(b) shows the L dependence of the peak shift of the $(00L)$ Bragg reflection from the average position $Q_c = (2\pi/d)L$, for the stage-2 $\text{Co}_c\text{Mn}_{1-c}\text{Cl}_2$ GIC's with $c = 0, 0.1, 0.7,$ and 0.85 , where L is the Bragg index number of stage 2. The PS for $c = 1.0$ and 0.4 is also shown in Figs. 1(b) and 2(b), respectively, for comparison with calculations. The PS in Figs. 4(b) and 2(b) has local maxi-

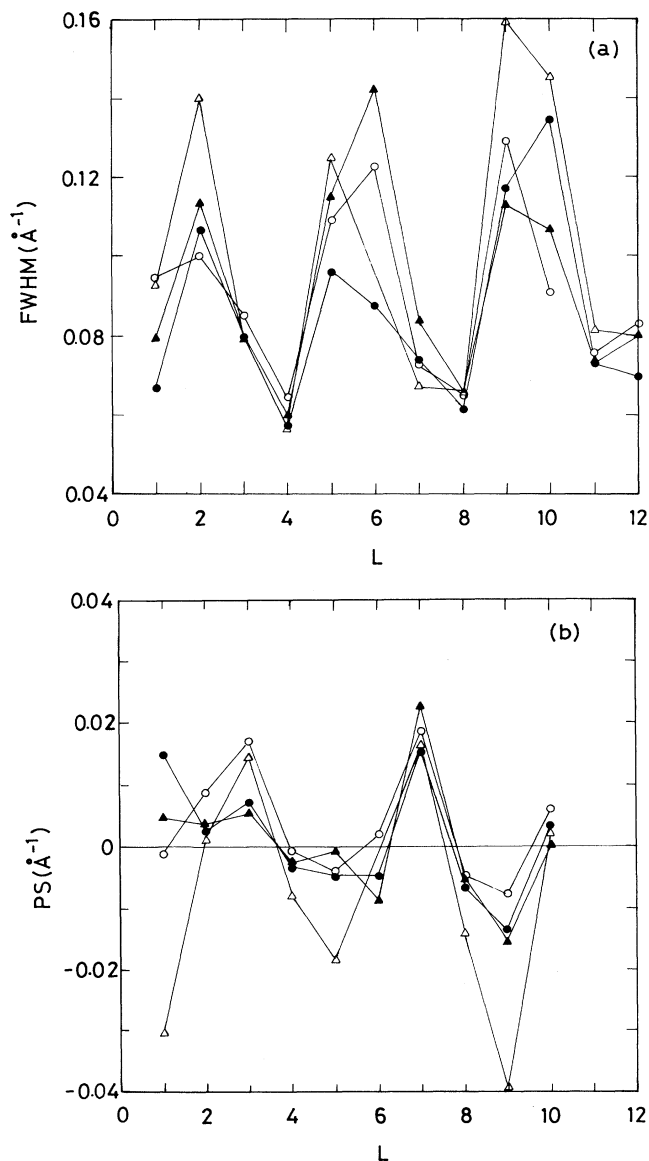


FIG. 4. L dependence of the (a) FWHM and (b) PS at 300 K for the stage-2 $\text{Co}_c\text{Mn}_{1-c}\text{Cl}_2$ GIC's with $c = 0$ (\circ), 0.1 (\bullet), 0.7 (\triangle), and 0.85 (\blacktriangle), where L is the Bragg index number of stage 2.

ma at $L = 3$ and 7 , and local minima at $L = 5$ and 9 , indicating a HT-type staging disorder with a stage-2 and stage-3 mixture for the samples with $c = 0, 0.1, 0.4, 0.7,$ and 0.85 . On the other hand, the PS in Fig. 1(b) has local minima at $L = 3$ and 7 , and local maxima at $L = 5$ and 9 , indicating a HT-type staging disorder with a stage-2 and stage-1 mixture for the sample with $c = 1.0$. The values of $f_1, f_2,$ and f_3 listed in Table II were obtained by comparing the data on the intrinsic FWHM and PS for each sample with theoretical calculations shown in Figs. 1 and 2. Note that the sample No. CM55 shows a phase separation of stage 2 and stage 1. It is found from Table II that the degree of the staging disorder for samples with $c \approx 0.5$ is much higher than that for samples with $c \approx 0$ and 1 .

The value of d spacing was determined from the least-squares fit of the Q_c value of Bragg peaks versus L and listed in Table II. Figure 5 shows the Co-concentration dependence of the value of the d spacing for the stage-2 $\text{Co}_c\text{Mn}_{1-c}\text{Cl}_2$ GIC's samples. The mean value of the d spacing seems to change linearly with the Co concentration from 12.893 \AA for $c = 0.0$ to 12.789 \AA for $c = 1.0$, supporting the empirical Vegard law in the stage-2 $\text{Co}_c\text{Mn}_{1-c}\text{Cl}_2$ GIC's. This result indicates that Co and Mn atoms are randomly distributed on the triangular lattice sites of the $\text{Co}_c\text{Mn}_{1-c}\text{Cl}_2$ intercalate layer. Very large experimental uncertainties in d are found around the mean value for several samples, including the CM60 sample. These experimental uncertainties of d arise from

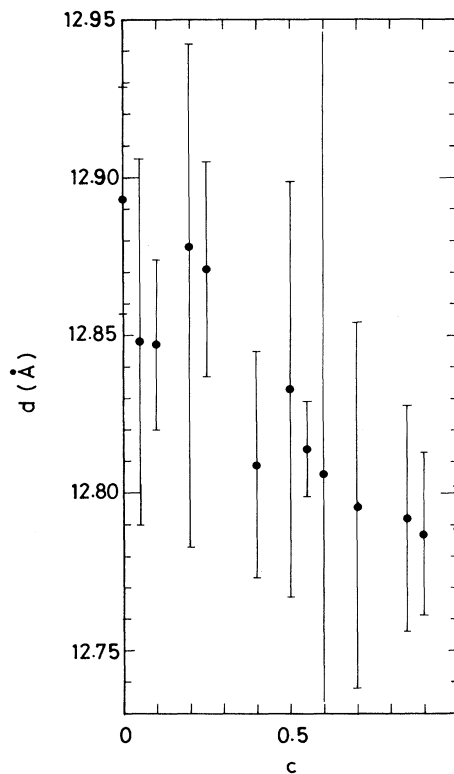


FIG. 5. c -axis repeat distance of stage-2 $\text{Co}_c\text{Mn}_{1-c}\text{Cl}_2$ GIC's at 300 K as a function of Co concentration c ($0 \leq c \leq 1.0$). The uncertainties in d are shown by error bars.

the oscillation of the PS with L . For example, as is listed in Table II, the CM60 and CM85 samples have the HT-type staging disorder with a stage-2 and -3 mixture: $f_2=0.6$ and $f_3=0.4$ for CM60, and $f_2=0.9$ and $f_3=0.1$ for CM85. The amplitude of the PS oscillation for CM60 is much larger than that for CM85: $\Delta_{PS}=0.071 \text{ \AA}^{-1}$ at $L=3$ and -0.109 \AA^{-1} at $L=9$ for CM60, and $\Delta_{PS}=0.006 \text{ \AA}^{-1}$ at $L=3$ and -0.016 \AA^{-1} at $L=9$ for CM85. The uncertainty in d for CM60 is much larger than that for CM85: $d=12.792\pm 0.036 \text{ \AA}$ for CM85 and $d=12.806\pm 0.241 \text{ \AA}$ for CM60. These results show that the experimental uncertainty in d increases with increasing amplitude of the PS oscillation.

B. Paramagnetic susceptibility

The dc magnetic susceptibility of the stage-2 $\text{Co}_c\text{Mn}_{1-c}\text{Cl}_2$ GIC's with $c=0, 0.1, 0.2, 0.25, 0.3, 0.4, 0.45, 0.55, 0.7, 0.8, 0.85, 0.9,$ and 1.0 was measured at $H=4.0$ kOe in the temperature range of $20 \leq T \leq 300$ K. The least-squares fit of the dc magnetic susceptibility data for $150 \leq T \leq 300$ K to the Curie-Weiss law

$$\chi_M = \frac{C_M}{T - \Theta} + \chi_M^0 \quad (11)$$

yields the values of the Curie-Weiss constant C_M (emu/average mol), the Curie-Weiss temperature Θ (K), and the temperature-independent susceptibility χ_M^0 . The values of C_M and Θ thus obtained are listed in Table III. Figure 6 shows a typical example of the reciprocal susceptibility $(\chi_M - \chi_M^0)^{-1}$ for $c=0.4$ as a function of temperature. The dc susceptibility is found to obey the Curie-Weiss law above 150 K. The deviation of the reciprocal susceptibility from the straight line below 150 K is due to the growth of spin short-range order. Figure 7 shows the Co concentration dependence of Θ for the stage-2 $\text{Co}_c\text{Mn}_{1-c}\text{Cl}_2$ GIC's. The value of Θ monotonically

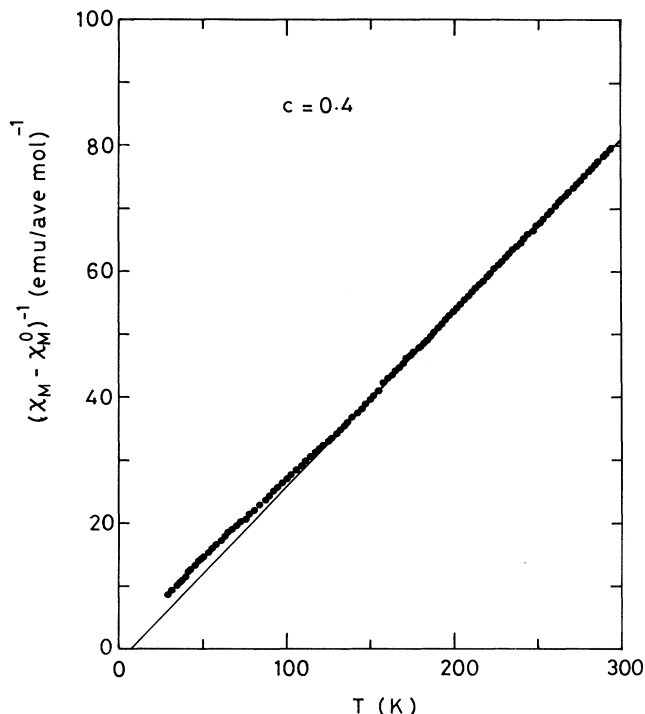


FIG. 6. Reciprocal susceptibility $(\chi_M - \chi_M^0)^{-1}$ vs temperature of stage-2 $\text{Co}_c\text{Mn}_{1-c}\text{Cl}_2$ GIC with $c=0.4$, where χ_M^0 is a temperature-independent susceptibility. The solid line is described by Eq. (11) with C_M , Θ , and χ_M^0 listed in Table III.

decreases as the Co concentration decreases, and changes its sign from positive to negative around $c \approx 0.2$, showing the change of magnetic behavior from ferromagnetic to antiferromagnetic. According to the molecular-field theory developed by Hashimoto¹⁹ and Yeh *et al.*,⁶ the Curie-Weiss temperature Θ is expressed by

$$\Theta = \frac{c^2 P^2(\text{Co})\Theta(\text{Co}) + (1-c)^2 P^2(\text{Mn})\Theta(\text{Mn}) + 2ac(1-c)\sqrt{[\Theta(\text{Co})\Theta(\text{Mn})]P(\text{Co})P(\text{Mn})}}{cP^2(\text{Co}) + (1-c)P^2(\text{Mn})}, \quad (12)$$

TABLE III. Curie-Weiss temperature Θ , Curie-Weiss constant C_M , average effective magnetic moment P_{eff} , and temperature-independent susceptibility χ_M^0 for the stage-2 $\text{Co}_c\text{Mn}_{1-c}\text{Cl}_2$ GIC's.

Sample name	c	Θ (K)	C_M (emu/average mol)	P_{eff} (μ_B /average mol)	χ_M^0 (10^{-3} emu/average mol)
No. CM00	0.0	-10.19 ± 0.77	4.55	6.04	-1.18 ± 0.09
No. CM10	0.1	-4.70 ± 0.51	4.42	5.95	-0.68 ± 0.07
No. CM20	0.2	-1.98 ± 0.31	4.49	5.99	0.003 ± 0.044
No. CM25	0.25	-0.05 ± 0.30	4.23	5.82	-0.07 ± 0.03
No. CM30	0.3	6.31 ± 0.28	3.55	5.33	0.55 ± 0.02
No. CM40	0.4	7.03 ± 0.23	3.60	5.37	-0.10 ± 0.02
No. CM45	0.45	9.83 ± 0.15	3.81	5.52	-0.006 ± 0.014
No. CM55	0.55	14.36 ± 0.19	3.80	5.51	-0.19 ± 0.01
No. CM70	0.70	16.15 ± 0.24	3.86	5.55	-0.31 ± 0.02
No. CM80	0.80	18.57 ± 0.22	3.91	5.59	0.12 ± 0.02
No. CM85	0.85	19.89 ± 0.15	4.07	5.70	-0.43 ± 0.01
No. CM90	0.90	24.38 ± 0.35	4.08	5.71	-0.85 ± 0.04
No. CM100	1.00	23.2	3.84	5.54	-0.085

where $P(\text{Co})$ and $P(\text{Mn})$ are the effective magnetic moments of stage-2 CoCl_2 and MnCl_2 GIC, respectively, and $\Theta(\text{Co})$ and $\Theta(\text{Mn})$ are the Curie-Weiss temperatures of stage-2 CoCl_2 and MnCl_2 GIC, respectively (Table I). Here α is a parameter defined by $\alpha = J(\text{Co-Mn}) / [J(\text{Co-Co})J(\text{Mn-Mn})]^{1/2}$, where $J(\text{Co-Co})$ ($=7.75$ K) and $J(\text{Mn-Mn})$ ($=-0.2$ K) are the intraplanar exchange interactions between Co^{2+} spins in the stage-2 CoCl_2 GIC and between Mn^{2+} spins in the stage-2 MnCl_2 GIC, respectively, and $J(\text{Co-Mn})$ is the intraplanar exchange interaction between Co and Mn spins. The data of Θ in Fig. 7 fit well to the solid line denoted by Eq. (12) with $\alpha=1.2$, indicating that $J(\text{Co-Mn})$ is ferromagnetic and is estimated as $J(\text{Co-Mn})=1.49$ K.

Our result that the average intraplanar exchange interaction changes from antiferromagnetic to ferromagnetic around $c \approx 0.2$ is simply explained as follows. When Co and Mn atoms are assumed to be randomly distributed on the triangular lattice of the $\text{Co}_c\text{Mn}_{1-c}\text{Cl}_2$ intercalate layer, the probability of finding the bonds of Co-Co, Mn-Mn, and Co-Mn in the intercalate layer is given by $p(\text{Co-Co})=c^2$, $p(\text{Co-Mn})=2c(1-c)$, and $p(\text{Mn-Mn})=(1-c)^2$, respectively. Then the average spin-pair energy is described by

$$\begin{aligned} E(i,j) = & -J(\text{Mn-Mn})(1-c)^2 \mathbf{S}_i(\text{Mn}) \cdot \mathbf{S}_j(\text{Mn}) \\ & -J(\text{Co-Mn})2c(1-c) \mathbf{S}_i(\text{Co}) \cdot \mathbf{S}_j(\text{Mn}) \\ & -J(\text{Co-Co})c^2 \mathbf{S}_i(\text{Co}) \cdot \mathbf{S}_j(\text{Co}), \end{aligned} \quad (13)$$

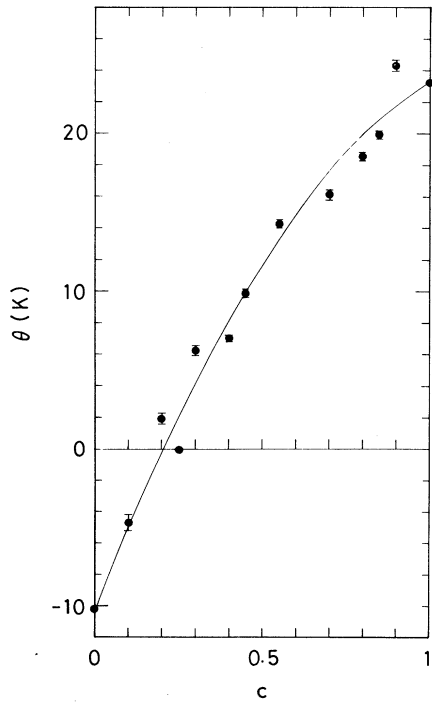


FIG. 7. Curie-Weiss temperature Θ vs Co concentration c for the stage-2 $\text{Co}_c\text{Mn}_{1-c}\text{Cl}_2$ GIC's. The solid line is described by Eq. (12) with $\alpha=1.2$.

where $|\mathbf{S}_i(\text{Mn})|^2 = \frac{5}{2}(\frac{5}{2}+1)$ and $|\mathbf{S}_i(\text{Co})|^2 = \frac{1}{2}(\frac{1}{2}+1)$. When the directions of $\mathbf{S}(\text{Mn})$ and $\mathbf{S}(\text{Co})$ are assumed to be limited to the $\pm x$ direction, it is found from Eq. (13) that $E(i,j)$ for the antiferromagnetic spin ordering is lower than that for the ferromagnetic spin ordering for $c < 0.24$ and $E(i,j)$ for the ferromagnetic spin ordering is lower than that for the antiferromagnetic spin ordering for $c > 0.24$. For $c=0.24$, $p(\text{Mn-Mn})$ is a little larger than $p(\text{Co-Mn})$, and $p(\text{Co-Co})$ is much smaller than $p(\text{Co-Mn})$. This suggests that the spin ordering of the system around $c=0.24$ is determined by the competition between antiferromagnetic $J(\text{Mn-Mn})$ and ferromagnetic $J(\text{Co-Mn})$.

Figure 8 shows the average effective magnetic moment P_{eff} of the stage-2 $\text{Co}_c\text{Mn}_{1-c}\text{Cl}_2$ GIC's as a function of Co concentration c , which is derived from the Curie-Weiss constant $C_M = N_A \mu_B^2 P_{\text{eff}}^2 / 3k_B$. Here N_A is Avogadro's number, μ_B is the Bohr magneton, and k_B is the Boltzmann constant. It is found from Fig. 8 that P_{eff} has a minimum value $5.33 \mu_B/\text{ave mol}$ around $c=0.3$. According to the molecular-field theory, the average effective magnetic moment P_{eff} is given by

$$P_{\text{eff}} = [cP_{\text{eff}}^2(\text{Co}^{2+}) + (1-c)P_{\text{eff}}^2(\text{Mn}^{2+})]^{1/2}, \quad (14)$$

when Co^{2+} and Mn^{2+} ions are randomly distributed in the magnetic intercalate layers. The solid line in Fig. 8 denotes the value of P_{eff} described by Eq. (14) with $P_{\text{eff}}(\text{Co}^{2+})=P(\text{Co})=5.54 \mu_B/\text{mol}$ and $P_{\text{eff}}(\text{Mn}^{2+})=P(\text{Mn})=6.04 \mu_B/\text{mol}$. The experimental data of P_{eff} greatly deviate from this solid line in the range of

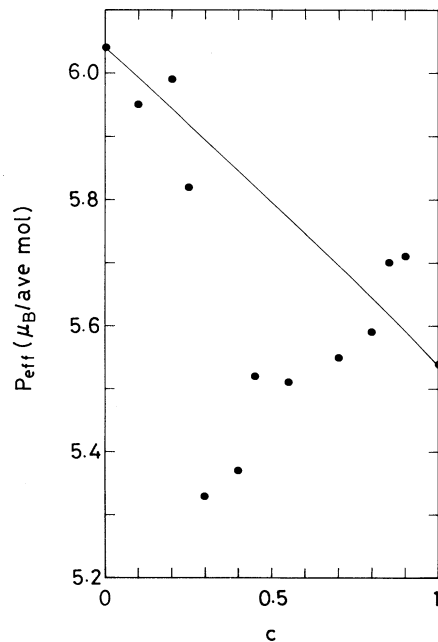


FIG. 8. Average effective magnetic moment P_{eff} ($\mu_B/\text{ave mol}$) as a function of Co concentration c for the stage-2 $\text{Co}_c\text{Mn}_{1-c}\text{Cl}_2$ GIC's. The solid line is described by Eq. (14).

$0.2 < c < 0.8$. This deviation may be due to a partial replacement of Mn^{2+} ions by M_i ($[M_i] = [\text{Mn}^{3+}]$ or $[\text{Mn}^+]$ or $([\text{Mn}^{3+}] + [\text{Mn}^-])/2$) ions. The value of P_{eff} for Mn^{3+} is assumed to be the same as that for Mn^{2+} because of the same total spin angular momentum: $S=2$. The value of P_{eff} is calculated as $P_{\text{eff}} = g[S(S+1)]^{1/2} = 4.9 \mu_B/\text{mol}$ for $S=2$ and $g=2$. For the case of $[M_i] = [\text{Mn}^+]$, charges may be transferred from the graphite layers to the inside of islands in the intercalate layers: $\text{Mn}^+ = \text{Mn}^{2+} + e^-$. For the case of $[M_i] = ([\text{Mn}^{3+}] + [\text{Mn}^+])/2$, charges may be transferred from the graphite layer to the periphery of the islands because of the charge neutrality inside the islands: $[\text{Mn}^{2+}] = ([\text{Mn}^{3+}] + [\text{Mn}^+])/2$. For the system consisting of Co^{2+} , Mn^{2+} , and M_i ions, the average effective magnetic moment P_{eff} is described by

$$P_{\text{eff}} = [cP_{\text{eff}}(\text{Co}^{2+}) + c_a P_{\text{eff}}(\text{Mn}^{2+}) + c_b P_{\text{eff}}(M_i)]^{1/2}, \quad (15)$$

where $P_{\text{eff}}(M_i) = 4.9 \mu_B/\text{mol}$, and c_a and c_b are the concentrations of Mn^{2+} and M_i , respectively ($c_a + c_b = 1 - c$). The Co concentration dependence of c_a and c_b is obtained from Eq. (15) by using the experimental data of P_{eff} : $P_{\text{eff}}(\text{Co}^{2+}) = P(\text{Co}) = 5.54 \mu_B/\text{mol}$ and $P_{\text{eff}}(\text{Mn}^{2+}) = P(\text{Mn}) = 6.04 \mu_B/\text{mol}$. Figure 9 shows the Co concentration dependence of c_a and c_b thus obtained. The concentration c_b is nearly equal to zero in the range

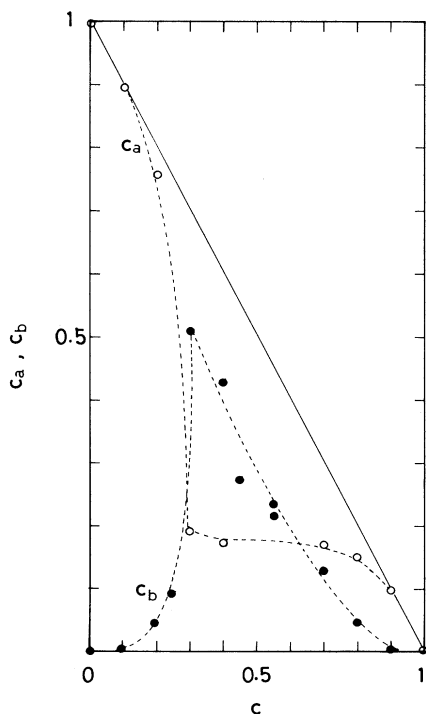


FIG. 9. Concentration of Mn^{2+} denoted by open circles and M_i ($[M_i] = [\text{Mn}^+]$ or $[\text{Mn}^{3+}]$ or $([\text{Mn}^+] + [\text{Mn}^{3+}])/2$) denoted by solid circles inside the magnetic intercalate layer of the stage-2 $\text{Co}_c\text{Mn}_{1-c}\text{Cl}_2$ GIC's, as a function of Co concentration. The dashed lines are guides to the eye.

of $0 \leq c \leq 0.1$ and $0.9 \leq c \leq 1.0$, indicating no replacement of Mn^{2+} by M_i . The concentration c_b rapidly increases around $c \approx 0.2$ and exhibits a sharp peak at $c = 0.3$, indicating a partial replacement of Mn^{2+} by M_i . For $0.3 \leq c \leq 0.8$, c_b monotonically decreases with increasing Co concentration, while c_a remains constant ($c_a = 0.18$).

Here we note that the experimental data of Θ is in excellent agreement with Eq. (12) with $\alpha = 1.2$ on the basis of the assumption that Co^{2+} and Mn^{2+} are randomly distributed in the $\text{Co}_c\text{Mn}_{1-c}\text{Cl}_2$ intercalate layer. This result indicates that the intraplanar exchange interactions $J(\text{Mn-Mn})$ and $J(\text{Co-Co})$ are not influenced by a partial replacement of Mn^{2+} by M_i .

C. Magnetic phase transition

Figure 10 shows the temperature dependence of dc magnetic susceptibility in the temperature range $1.5 \leq T \leq 18$ K for stage-2 $\text{Co}_c\text{Mn}_{1-c}\text{Cl}_2$ GIC's with (a) $c = 0, 0.1, \text{ and } 0.2$ ($H = 340$ Oe); (b) $c = 0.3$ and 0.4 ($H = 340$ Oe); and (c) $c = 0.45, 0.55, 0.7, 0.8, 0.9, \text{ and } 1.0$ ($H = 100$ Oe). Figure 11 shows the Co concentration dependence of the dc magnetic susceptibility at 5 K obtained from Fig. 10. It is found from Fig. 11 that (i) the dc magnetic susceptibility has a very small value below $c \approx 0.3$, (ii) it rapidly increases around $c \approx 0.4$, and (iii) it monotonically increases as the Co concentration increases for $c > 0.5$. These results suggest that the magnetic behavior of the system changes from antiferromagnetic to ferromagnetic around $c \approx 0.3$. No hysteresis between a field-cooled (FC) and zero-field-cooled (ZFC) dc magnetic susceptibilities is observed for $H = 340$ Oe around $0 \leq c \leq 0.3$. This result indicates two possibilities: (i) that a spin-glass phase does not exist or (ii) that the spin-glass phase is destroyed by the application of a magnetic field ($H = 340$ Oe). The possibility (i) is ruled out because the magnetic behaviors of the stage-2 MnCl_2 GIC ($c = 0$) below T_N are found to be similar to those of the spin-glass phase.¹⁴ (1) The susceptibilities χ' and χ'' show sharp cusps around $T_N = 1.1$ K for $H = 0$. (2) The position of the peak in χ' shifts to the lower temperature side with decreasing frequency. (3) A hysteresis between the FC and ZFC magnetizations measured for $H = 100$ mOe is observed below T_N . These behaviors may be due to a spin frustration effect which occurs inside the MnCl_2 intercalate layers because of the fully frustrated nature of the 2D antiferromagnet on the triangular lattice sites. For $c \approx 0.24$ another spin frustration effect is expected to arise from a competition between the antiferromagnetic interaction $J(\text{Mn-Mn})$ and the ferromagnetic interaction $J(\text{Co-Mn})$.¹⁰ These two kinds of the spin frustration effects are expected to give rise to the spin-glass phase in the low-Co-concentration region. In the present work the dc magnetic susceptibility measurement for $H < 340$ Oe has not been conducted because of low sensitivity in our Faraday balance method. The possibility of the spin-glass phase for $0 < c < 0.3$ can be examined by using ac susceptibility and dc magnetic susceptibility in the presence of very weak magnetic field.

The dc magnetic susceptibility data for $c \geq 0.4$ shown in Figs. 10(b) and 10(c) are described by

$M/H = \chi_M + M_0/H$, where M_0 is proportional to a saturation magnetization of the ferromagnetic systems. As the temperature decreases below a critical temperature T_c , the second term (M_0/H) becomes dominant because of the appearance of long-range spin ordering below T_c .

The temperature dependence of the dc magnetic susceptibility is almost the same as that of the spontaneous magnetization. It is found from Fig. 10(c) that the dc magnetic susceptibility data show tails around T_c because of a smearing of T_c arising from (i) the macroscopic gradient

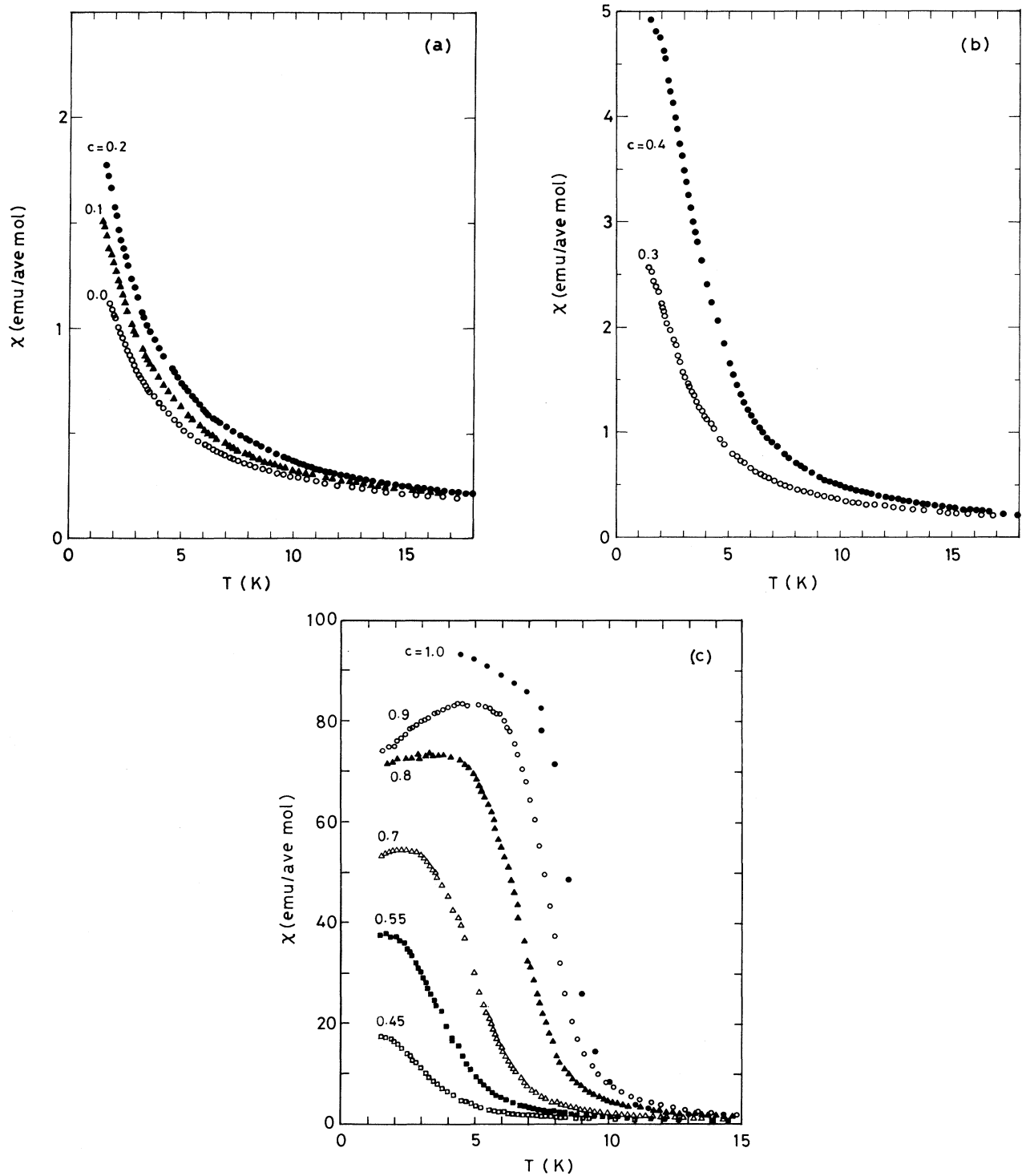


FIG. 10. dc magnetic susceptibility of stage-2 $\text{Co}_c\text{Mn}_{1-c}\text{Cl}_2$ GIC's at low temperatures. (a) $c=0, 0.1$, and 0.2 ($H=340$ Oe and $H1c$). (b) $c=0.3$ and 0.4 ($H=340$ Oe and $H1c$). (c) $c=0.45, 0.55, 0.7, 0.8, 0.9$, and 1.0 ($H=100$ Oe and $H1c$).

of the Co concentration over the sample and (ii) the finite-size effect. When the distribution of the critical temperature is assumed to be governed by a Gaussian distribution function $f(T_c)$ with average critical temperature $\langle T_c \rangle$ (K) and width σ (K), the magnetization can be expressed by a power law with a critical exponent β

$$M(T) = A \int_T^\infty \left[1 - \frac{T}{T_c} \right]^\beta f(T_c) dT_c, \quad (16)$$

where A is a constant. The least-squares fit of the dc magnetic susceptibility data of Figs. 10(b) and 10(c) to Eq. (16) yields the value of $\langle T_c \rangle$, σ , and β listed in Table IV for the stage-2 $\text{Co}_c\text{Mn}_{1-c}\text{Cl}_2$ GIC's with $c=0.40, 0.45, 0.55, 0.7, 0.8, 0.85, 0.9, \text{ and } 1.0$.

Figure 12 shows the Co concentration dependence of the average critical temperature $\langle T_c \rangle$. In this figure also shown is the Néel temperature T_N of the stage-2 MnCl_2 GIC ($T_N=1.1$ K), which has been determined from ac susceptibility measurements.^{13,14} The value of $\langle T_c \rangle$ at $c=1.0$ ($\langle T_c \rangle=8.78$ K) is close to the value of T_{cu} listed in Table I ($=9.1$ K). The average critical temperature $\langle T_c \rangle$ rapidly decreases as c decreases from $c=1.0$ to 0.55 ($\langle T_c \rangle=3.724$ K at $c=0.55$), but does not reduce to zero even below the percolation threshold $c=0.5$ predicted for the 2D triangular lattice because of the ferromagnetic interaction $J(\text{Co-Mn})$ and the antiferromagnetic $J(\text{Mn-Mn})$. The phase diagram of Fig. 12 indicates that for $c \geq 0.45$ the phase transition occurs between the low-temperature ferromagnetic phase and the high-

TABLE IV. Critical exponent β , the distribution of the critical temperature σ (K) and the average of critical temperature $\langle T_c \rangle$ (K) for the stage-2 $\text{Co}_c\text{Mn}_{1-c}\text{Cl}_2$ GIC's.

Sample name	c	β	σ (K)	$\langle T_c \rangle$ (K)	$\sigma/\langle T_c \rangle$
No. CM40	0.40	0.137	1.079	3.845	0.2806
No. CM45	0.45	0.060	1.106	3.346	0.3305
No. CM55	0.55	0.107	0.595	3.724	0.1598
No. CM70	0.70	0.046	1.222	5.290	0.2310
No. CM80	0.80	0.085	1.119	7.029	0.1591
No. CM85	0.85	0.040	0.883	5.781	0.1527
No. CM90	0.90	0.085	0.893	7.989	0.1118
No. CM100	1.00	0.082	0.620	8.780	0.0706

temperature paramagnetic phase. The critical exponent β is found to lie between 0.04 for $c=0.85$ and 0.137 for $c=0.4$. The universality to which these systems belong is not uniquely determined from the value of β obtained for each Co concentration, although these systems are assumed to have the 2D XY symmetry because of the XY anisotropy in the stage-2 CoCl_2 and MnCl_2 GIC.

The width σ of the Gauss distribution function is described by $\sigma=(\sigma_s^2+\sigma_c^2)^{1/2}$, where σ_s and σ_c are the smearing of the critical temperature due to the finite-size effect and the macroscopic gradient of Co concentration

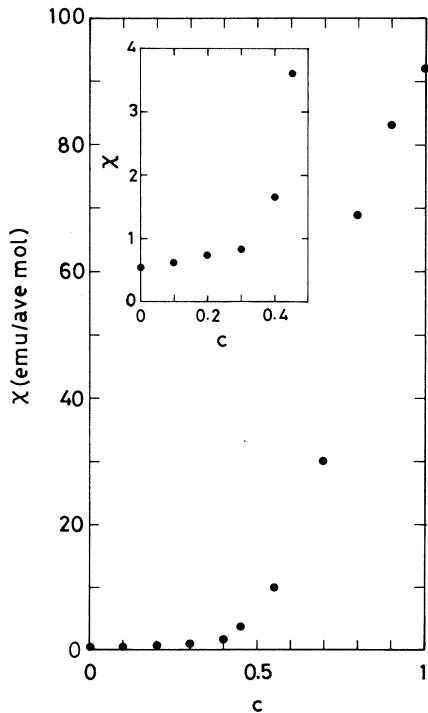


FIG. 11. dc magnetic susceptibility as a function of Co concentration c at $T=5$ K for the stage-2 $\text{Co}_c\text{Mn}_{1-c}\text{Cl}_2$ GIC's.

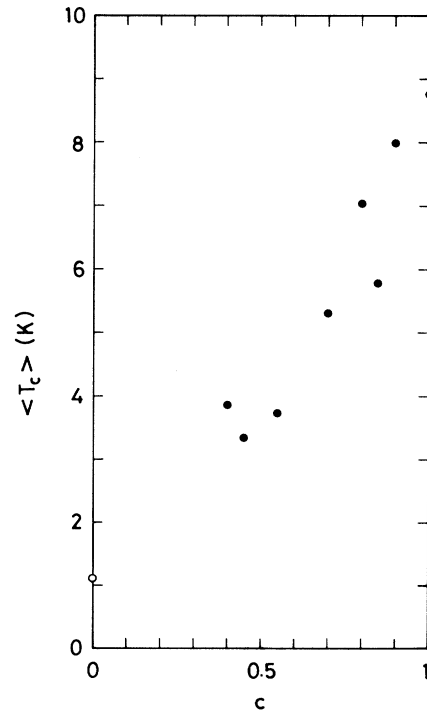


FIG. 12. Co concentration dependence of the average critical temperature $\langle T_c \rangle$ of stage-2 $\text{Co}_c\text{Mn}_{1-c}\text{Cl}_2$ GIC's. The open circle denotes $T_N=1.1$ K for the stage-2 MnCl_2 GIC (Refs. 13 and 14).

over the sample, respectively. According to finite-size scaling,²⁰ the ratio $\sigma_s/\langle T_c \rangle$ is described by $\sigma_s/\langle T_c \rangle \sim d_s^{-1/\nu}$, where d_s is island diameter and ν is the critical exponent of the spin correlation length. The ratio $\sigma_s/\langle T_c \rangle$ is considered to be independent of c because of the same order of d_s for any c . Since the ratio $\sigma_c/\langle T_c \rangle$ at $c=1.0$ is assumed to be equal to zero, the value of $\sigma_s/\langle T_c \rangle$ for any c is given by the value of $\sigma/\langle T_c \rangle$ at $c=1.0$ ($=0.07$). Then the ratio $\sigma_c/\langle T_c \rangle$ is found to increase from 0 to 0.32 as the Co concentration decreases from $c=1$ to 0.45. This result suggests that the macroscopic gradient of Co concentration over the sample increases with decreasing the Co concentration and has a maximum around $c=0.5$.

VI. CONCLUSION

The stage-2 $\text{Co}_c\text{Mn}_{1-c}\text{Cl}_2$ GIC's approximate two-dimensional site-random XY spin systems having both ferromagnetic $J(\text{Co-Co})$ and antiferromagnetic $J(\text{Mn-Mn})$ intraplanar exchange interactions inside the $\text{Co}_c\text{Mn}_{1-c}\text{Cl}_2$ intercalate layers. The Co and Mn ions

are randomly distributed on the triangular lattice sites. The phase diagram determined from the dc magnetic susceptibility indicates a ferromagnetic phase for $c \geq 0.45$. The intraplanar exchange interaction between Co and Mn ions is ferromagnetic: $J(\text{Co-Mn})=1.49$ K. There is a possibility of a spin-glass phase around $c \approx 0.24$ because of a competition between $J(\text{Mn-Mn})$ and $J(\text{Co-Mn})$. No evidence for the spin-glass phase has been found from the dc magnetic susceptibility for $0 \leq c \leq 0.4$ at $H \geq 340$ Oe. The possibility of the spin-glass phase in the low Co concentration will be examined using ac susceptibility in the presence of a very weak magnetic field.

ACKNOWLEDGMENTS

We would like to thank H. Suematsu and Y. Hishiyama for providing us with good-quality single-crystal Kish graphites. We are grateful to W. Zhang, L. H. Chang, and W. Brinkman for their help on the dc magnetic susceptibility measurement. This work was supported by National Science Foundation Grant No. DMR-8902351.

- ¹H. Zabel and P. C. Chow, *Comments Condens. Matter Phys.* **12**, 225 (1986).
- ²G. Dresselhaus, J. T. Nicholls, and M. S. Dresselhaus, in *Graphite Intercalation Compounds II*, edited by H. Zabel and S. A. Solin (Springer-Verlag, Berlin, 1990).
- ³M. Suzuki, *CRC Crit. Rev. Solid State Mater. Sci.* **16**, 237 (1990).
- ⁴D. G. Wiesler, M. Suzuki, and H. Zabel, *Phys. Rev. B* **36**, 7051 (1987).
- ⁵J. S. Speck and M. S. Dresselhaus, *Synth. Metals* **34**, 211 (1989).
- ⁶M. Yeh, M. Suzuki, and C. R. Burr, *Phys. Rev. B* **40**, 1422 (1989).
- ⁷M. Yeh, I. S. Suzuki, M. Suzuki, and C. R. Burr, *J. Phys. Condens. Matter* **2**, 9821 (1990).
- ⁸J. T. Nicholls and G. Dresselhaus, *Phys. Rev. B* **41**, 9744 (1990).
- ⁹M. Suzuki, L. F. Tien, I. S. Suzuki, and C. R. Burr, *J. Appl.*

- Phys.* **67**, 5749 (1990).
- ¹⁰K. Katsumata, J. Tuchendler, Y. J. Uemura, and H. Yoshizawa, *Phys. Rev. B* **37**, 356 (1988).
- ¹¹S. Hendricks and E. Teller, *J. Chem. Phys.* **10**, 147 (1942).
- ¹²D. G. Wiesler, M. Suzuki, P. C. Chow, and H. Zabel, *Phys. Rev. B* **34**, 7951 (1986).
- ¹³Y. Kimishima, A. Furukawa, M. Suzuki, and H. Nagano, *J. Phys. C* **19**, L43 (1986).
- ¹⁴M. Matsuura, Y. Karaki, T. Yonezawa, and M. Suzuki, *Jpn. J. Appl. Phys.* **26**, Suppl. **26-3**, 773 (1987).
- ¹⁵D. Hohlwein and W. Metz, *Z. Kristallogr.* **139**, 279 (1974).
- ¹⁶M. E. Huster, P. A. Heiney, V. B. Cajipe, and J. E. Fischer, *Phys. Rev. B* **35**, 3311 (1987).
- ¹⁷J. Kakinoki and Y. Komura, *J. Phys. Soc. Jpn.* **7**, 30 (1952).
- ¹⁸I. S. Suzuki and M. Suzuki (unpublished).
- ¹⁹T. Hashimoto, *J. Phys. Soc. Jpn.* **18**, 1140 (1963).
- ²⁰M. E. Fisher and A. E. Ferdinand, *Phys. Rev. Lett.* **19**, 169 (1967).